



Theoretical and experimental investigation into anti-idling A/C system for trucks



F. Bagheri^{*}, M.A. Fayazbakhsh, P. Cheppudira Thimmaiah, M. Bahrami^{*}

Laboratory for Alternative Energy Conversion (LAEC), School of Mechatronic Systems Engineering, Simon Fraser University, Surrey, BC V3T 0A3, Canada

ARTICLE INFO

Article history:

Received 19 November 2014

Accepted 31 March 2015

Available online 10 April 2015

Keywords:

Air conditioning & refrigeration

Anti-idling

Optimum COP

ABSTRACT

In this study, a recently developed truck anti-idling air conditioning (A/C) system is investigated. A mathematical model is developed to simulate the thermodynamic and heat transfer characteristics of the A/C system and calculate the coefficient of performance (COP). Utilizing environmental chambers and a number of measuring equipment, an experimental setup is built to verify the accuracy of the mathematical model and to perform a comprehensive study on the performance of the system for a wide range of operating conditions. A good agreement between the simulation and the experimental data, with a maximum discrepancy of 10.6%, is achieved. The results show a range of 0.5–1.7 for the system COP under a variety of operating condition. The parametric study shows that for any cooling demand, ambient and indoor air temperatures, there is a point of optimum COP that can be achieved by adjusting the condenser and evaporator fans speed.

© 2015 Elsevier Ltd. All rights reserved.

1. Introduction

Idling vehicle engines, which is defined as running the engine while the vehicle is not moving, to power the auxiliaries, consumes a tremendous amount of energy leading to large quantities of greenhouse gas emissions (GHG). Long-haul trucks often idle overnight for 6–16 h to keep the driver comfortable while resting [1,2]. When the engine is running at idle condition, it takes a rich mixture of air and fuel, such that the fuel consumption rate is high. Additionally, during idling, the engine is not able to work at peak operating temperature and the combustion of fuel is incomplete that leaves fuel residues in the exhaust and thus, emission levels increase. On average, truck engines run at 30% thermal efficiency throughout highway operation, but at only 3–11% efficiency during idling [3–6]. For passenger vehicles across a wide range of sizes, the idling fuel consumption was shown to vary in a range of 0.7–1.9 lit/h. The commercial truck idling results in an average maintenance cost of \$0.12/h in addition to 2.3–7.6 lit/h fuel consumption that uses over 8% of the total fuel [2,7]. In the U.S., idling consumes about 6 billion gallons of oil per year, costing about \$20 billion [7].

Gaines et al. [2] tested a late-model mid-sized car (2011 Ford Fusion) for idling disadvantages at 21 °C ambient conditions and by considering all the effects of engine restart/warm-up and catalyst cooling, they showed that idling for more than 10 s uses more

fuel and emits more CO₂ than restarting the engine. Truck idling alone stands for half of the total idling consumption globally. Idling emissions of a truck engine can be as high as 86.4 g/h, 16,500 g/h, 5130 g/h, 4 g/h, and 375 g/h for HC, CO₂, CO, particulate matter (PM), and NO_x, respectively [3]. Only in the U.S., truck idling causes emissions of more than 130 tons of PM, 12 million tons of CO₂, 35,000 tons of NO_x, and 36,000 tons of CO each year [7]. Based on an average truck's engine idle power of 50–75 kW, an average of 2–4 kW power draw by the air conditioning system stands for 4–8 percent of the total idling GHG emission [8–11]. Accordingly, an average amount of 5.2 g/h, 990 g/h, 308 g/h, 0.24 g/h, and 22.5 g/h for HC, CO₂, CO, PM, and NO_x is generated by the truck engine only due to the air conditioning system operation; however, in most of the idling period the only purpose of running the engine is for air conditioning purpose.

In response to the increasing awareness of the adverse effects of idling engines on human health and the environment, many cities around the world have instituted idling restrictions and bans. Idling reduction efforts have focused on heavy-duty diesel vehicles because they are typically idled for extended periods. Currently in the U.S., engine idling is prohibited in 18 states and the idling-related legislation is propagating throughout north America [2,7]. Switzerland has laws that require motorists to turn off their engines while waiting for the red traffic light to turn green. England and Scotland likewise impose fines for engine idling violations while different countries like Canada, Italy, France, Germany,

^{*} Corresponding authors.

E-mail addresses: fbagheri@sfu.ca (F. Bagheri), mbahrami@sfu.ca (M. Bahrami).

Nomenclature

| | | | |
|-------------------|---|----------------------|------------------------------|
| COP | coefficient of performance | f | fan |
| c_0 to c_8 | compressor polynomial constants | $cond$ | condenser |
| d_0 to d_8 | compressor polynomial constants | $evap$ | evaporator |
| cf_0 to cf_3 | fan power consumption constants | $comp$ | compressor |
| C | thermal capacity ($W/^\circ C$) | TEV | thermostatic expansion valve |
| C^* | thermal capacity ratio (C_{min}/C_{max}) | E | electrical |
| g_1 to g_{20} | equation form | M | mechanical |
| h | enthalpy ($kJ/kg\ ^\circ C$) | in | inlet |
| \dot{m} | mass flow rate (kg/s) | out | outlet |
| W | power consumption (kW) | max | maximum |
| NTU | number of transfer units | min | minimum |
| \dot{Q} | heat transfer rate (W) | ref | refrigerant |
| T | temperature ($^\circ C$) | nom | nominal |
| P | pressure (kPa) | | |
| UA | heat exchanger overall heat transfer coefficient ($W/^\circ C$) | <i>Superscripts</i> | |
| x_1 to x_{20} | variables | n | iteration step number |
| <i>Subscripts</i> | | <i>Greek letters</i> | |
| a | air | ε | heat exchanger effectiveness |
| c | condensing | η | efficiency |
| e | evaporating | | |

Holland, Hong Kong, Taiwan, Japan and Singapore, regulates different idling time limits [12].

The idling limitation has caused a major difficulty for truck drivers and created a great demand for green anti-idling air conditioning (A/C) systems [13]. MacDonald et al. [13] generally assessed alternative anti-idling A/C systems that can respond to this demand. They concluded that the battery powered A/C systems are one of the promising alternatives toward eliminating engine idling. Due to the potential impact of anti-idling A/C systems on the global fuel consumption and environment, a performance evaluation and comprehensive parametric study on these systems is required.

Although there are numerous studies in the literature focused on A/C system in different applications, the number of studies relevant to general category of vehicle air conditioning (VAC) systems is restricted [14–20]. A majority of the studies in the field of VAC systems is related to assessment of refrigerant type effects on the characteristic and the performance [20–24]. A variety of other important parameters including: refrigerant charge, compressor speed, and ambient temperature have also been considered through the VAC system studies. Ratts and Brown [25] experimentally analyzed the coefficient of performance (COP) of a passenger car A/C system focusing on relationships between the COP, the compressor revolution, and the vehicle speed. Their analysis showed that the performance of the system degraded with increasing the vehicle speed. Wang et al. [26] experimentally showed that the COP of an VAC system decreased with increment of the refrigerant charge, condensing temperature and compressor speed, and increased with increment of the evaporator air inlet temperature. They reported the value of COP in the range of 1.1–2.5 for a variety of operating condition. Macagnan et al. [27] experimentally investigated into the effects of refrigerant charge and compressor speed on the cooling power and performance of a typical VAC and showed that although the refrigerant charge did not sensibly affect the VAC system characteristics, the compressor speed caused a variation of the system COP in a range of 1–1.8.

Alkan and Hosoz [28] experimentally compared a variable capacity compressor (VCC) and a fixed capacity compressor (FCC) for an VAC system in different engine rotational speeds as well as evaporator and condenser air stream characteristics. It was

shown that although the COP of VCC system during low engine rpm operations is slightly poorer, it surpasses the COP of FCC system at higher rpms. Moreover, the COP of FCC system decreases persistently with the compressor speed increment. Jabardo et al. [29] studied the effects of compressor speed and the evaporator and condenser inlet air temperatures on the performance of a VAC by developing a steady state thermodynamic simulation model. The transient behavior of an VAC system was studied by Tian and Li [4] using a quasi-steady state model. Also, the effects of refrigerant charge and condenser size on the performance of a typical VAC was studied by Lee and Yoo [19] based on a mathematical model.

In addition, a variety of innovative technologies to increase the energy efficiency of the VAC systems has been introduced in the open literature. Waste-heat driven air conditioning systems, which operate based on absorption or adsorption cycles, have been introduced in several studies as one of the promising future sustainable energy VAC systems [30–32]. Also, employing the microchannel condensers as a performance enhancement technology for VAC systems is covered in Ref. [33]. Muller [34] introduced the feasibility of employing magnetocaloric cooling for automotive industry. Gould et al. [35] studied the effects of capturing waste heat from the internal combustion engine exhaust to run steam pressure exchange ejector air conditioning system for an automobile. Ünal and Yilmaz [36] investigated into the effects of using two-phase ejectors as the expansion valve in air conditioning system of the buses and showed that a potential of 15% performance improvement can be achieved.

The presented literature review indicates that the performance evaluation of anti-idling A/C systems has not been studied in-depth, and the pertinent literature lacks the following:

- Performance evaluation of anti-idling A/C systems under realistic operating conditions.
- Comprehensive parametric study on the performance characteristics of A/C systems equipped to variable speed fans to find optimum COP for different ambient conditions.

The present study aims to develop a new mathematical model as well as an experimental setup for investigation into the

performance characteristics of a recently generated battery-powered truck anti-idling A/C unit. The study includes a comprehensive performance evaluation of the unit toward finding optimum condenser and evaporator air flow rates for each realistic ambient condition. The results can be used to develop an intelligent control module to adjust the fans speed of anti-idling A/C system for optimum operation at each ambient condition. Accordingly, the mathematical modeling and experimental study are both covered in this study for a comprehensive performance evaluation of a typical anti-idling A/C system. Fig. 1 shows a typical truck anti-idling A/C system that is utilized in this study. The system is formed of a condensing unit, an evaporating unit, a battery box, and refrigerant pipelines.

The condensing unit, which is installed outside on the rear wall of the truck cabin, consists of a scroll compressor model YWXD15 with $15 \text{ cm}^3/\text{rev}$ displacement manufactured by Nanjing Yinmao Compressor Co., a 12 V axial fan with $0.236 \text{ m}^3/\text{s}$ nominal flow rate, a receiver, a 2 row 14 fin/inch aluminum finned-tube coil, and a power control unit. The evaporating unit, which is installed inside the truck cabin, is built using a 3 row 14 fin/inch aluminum finned-tube coil, a centrifugal fan with $0.038 \text{ m}^3/\text{s}$ nominal flow rate, a thermostatic expansion valve (TEV), and manual temperature set point and air speed controls. The system is powered by a package of two 12 V batteries directly charged by the engine alternator. Normally, 0.79 kg of HFC-134a is charged into the system as the refrigerant.

2. Mathematical model

In this section a new mathematical model is developed for evaluating the performance of anti-idling truck A/C system and to simulate thermodynamic parameters under various working conditions. The major output parameter from the modeling of an A/C system is the coefficient of performance ($\text{COP} = \text{cooling power}/\text{input power}$). In addition to the COP, other parameters of an A/C

system, including: cooling power, input power, and refrigerant mass flow rate are obtained from the modeling results.

2.1. Compressor sub-model

A map-based model is used in this study for thermodynamic simulation of the compressor. It was experimentally shown that this approach had a good agreement with experimental data [37]. Second-order polynomial were developed for the compressor input power and refrigerant mass flow rate quantities based on the manufacturer's test data, as shown through Eqs. (1) and (2) in Table 1. These equations yield a maximum of 2.5% discrepancy when compared to the manufacturer's data. It should be noted that the manufacturer's data is usually provided for a fixed superheat and subcooled magnitudes. If the A/C system is equipped to a thermostatic expansion valve, the refrigerant flow rate is controlled to achieve a preset superheat amount. Accordingly, throughout the duty cycle the degree of refrigerant's superheat at the outlet of evaporator will be kept nearly constant. However, the subcooled degree will change depending upon the imposed condition on the system from the air-side. Therefore, a modification will be required for different superheat and subcooled degrees. In the current study, wide ranges of superheat and subcooled temperatures ($0\text{--}15 \text{ }^\circ\text{C}$) are tested and the modified correlations of the compressor model under different superheat and subcooled values are obtained and added. The refrigerant side thermodynamic correlation for the compressor is also presented in Eq. (3), see Table 1. Based on these equations, with known inlet conditions, the state point of the refrigerant gas at the compressor discharge can be calculated.

2.2. Condenser and evaporator models

Energy balance correlations between the refrigerant and air flows in condenser and evaporators are used to model heat transfer in these components. In the present study, following [38], an

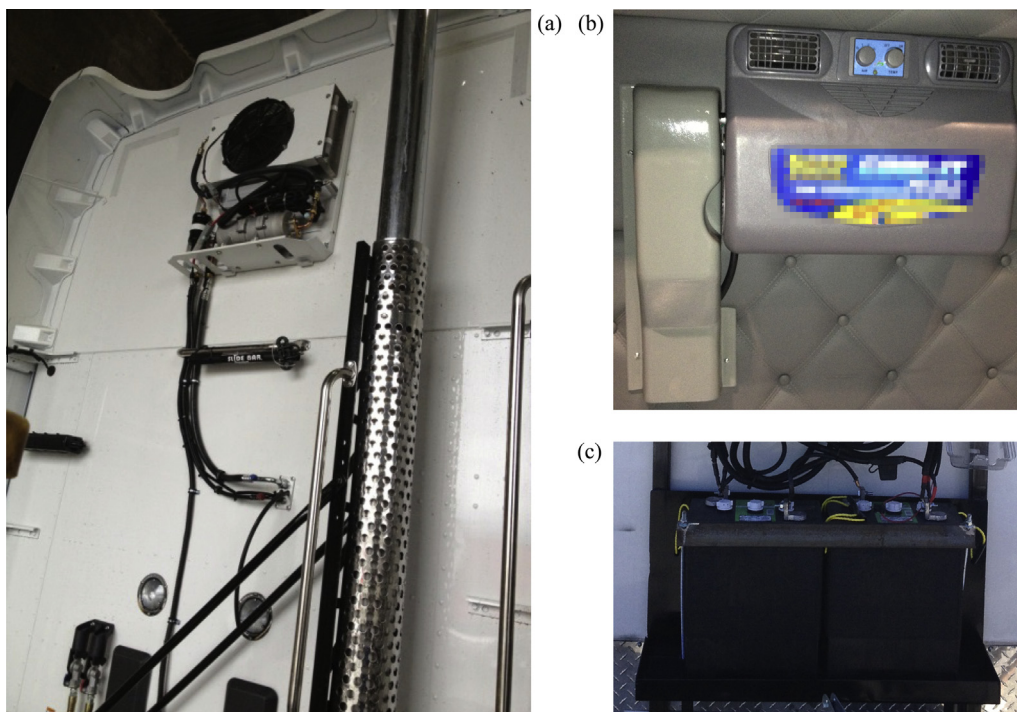


Fig. 1. Typical battery-powered anti-idling truck A/C: (a) condensing unit and connections on the rear wall of the truck cabin, (b) evaporating unit inside the truck cabin, and (c) batteries.

Table 1
Mathematical model correlations.

| | | |
|------------------------------------|---|------|
| Compressor sub-model | $W_{comp} = c_0 + c_1 T_e + c_2 T_c + c_3 T_e^2 + c_4 T_e T_c + c_5 T_c^2 + c_6 T_e^2 T_c + c_7 T_e T_c^2 + c_8 T_e^2 T_c^2$ | (1) |
| | $\dot{m}_{ref} = d_0 + d_1 T_e + d_2 T_c + d_3 T_e^2 + d_4 T_e T_c + d_5 T_c^2 + d_6 T_e^2 T_c + d_7 T_e T_c^2 + d_8 T_e^2 T_c^2$ | (2) |
| | $\dot{m}_{ref}(h_{ref,comp,out} - h_{ref,comp,in}) = W_{comp} \times \eta_E \times \eta_M$ | (3) |
| Condenser and evaporator sub-model | $\varepsilon = \dot{Q} / \dot{Q}_{max}$ | (4) |
| | $\dot{Q}_{max} = C_{min}(T_{hot,in} - T_{cold,in})$ | (5) |
| | $\dot{Q} = \varepsilon C_{min}(T_{hot,in} - T_{cold,in})$ | (6) |
| | $\varepsilon = 1 - \exp[-NTU(1 - C^*)] / (1 - C^* \exp[-NTU(1 - C^*)])$ | (7) |
| | $C^* = C_{min} / C_{max}, \quad NTU = UA / C_{min}$ | (8) |
| | $\dot{Q} = \dot{m}_a(h_{a,in} - h_{a,out}) $ | (9) |
| | $\dot{Q} = \dot{m}_{ref}(h_{ref,out} - h_{ref,in}) $ | (10) |
| | $W_f = W_{f,nom} \left(cf_0 + cf_1 \left(\frac{\dot{m}_a}{\dot{m}_{a,nom}} \right) + cf_2 \left(\frac{\dot{m}_a}{\dot{m}_{a,nom}} \right)^2 + cf_3 \left(\frac{\dot{m}_a}{\dot{m}_{a,nom}} \right)^3 \right)$ | (11) |
| Expansion valve sub-model | $h_{ref,TEV,in} = h_{ref,TEV,out}$ | (12) |

$\varepsilon - NTU$ model is employed to derive the mathematical model for the condenser and evaporator. In this approach, the effectiveness ε is defined as the ratio of the actual heat transfer to the maximum possible heat transfer, which Eq. (4), see Table 1. The maximum possible heat transfer is defined in Eq. (5). The actual heat transfer between the air stream and refrigerant flow can be calculated using Eq. (6). To use this equation, ε is required to be found from Eqs. (7) and (8). For the selected anti-idling A/C system, the condenser and evaporator specifications are obtained from the manufacturer data. In addition to the $\varepsilon - NTU$ correlations, which represents the heat transfer between the air and refrigerant streams, correlations of enthalpy change for both the refrigerant and air streams should be added to complete the heat transfer model for the evaporator and condenser. Eqs. (9) and (10) represent the enthalpy change respectively for the air and refrigerant streams in the condenser and evaporator. For the air stream in the evaporator, the enthalpy is calculated based on the temperature and relative humidity to include both the sensible and latent heat transfers. However, for the air stream in condenser, the enthalpy of air can be simply found using the temperature and thermal capacity of air since there is no water condensation on the condenser coil. It should be mentioned that two heat transfer regimes exist in the evaporator which are (1) two-phase heat transfer relevant to saturated zone and (2) single-phase heat transfer relevant to superheated zone. Also, the condenser can be divided into three heat transfer regimes which are single-phase superheated, two-phase saturated, and single-phase subcooled. Due to governance of different convective heat transfer equations for the mentioned regimes, in this study the evaporator and condenser are divided into two and three sub-zones, respectively. Thus, the $\varepsilon - NTU$ model is applied for each sub-zone separately to achieve a high level of accuracy. In addition to the heat transfer model for the condenser and evaporator, map-based correlations are employed to obtain the fans power consumption using manufacturer's datasheets [39], see Eq. (11) in Table 1.

2.3. Thermostatic expansion valve model

Following [37], an isenthalpic model is selected for thermodynamic simulation of the thermostatic expansion valve in the present study. In this model, as a result of adiabatic assumption, the inlet and outlet refrigerant enthalpies are considered the same, see Eq. (12).

2.4. Numerical solver

Developing the mathematical model for anti-idling truck A/C system, including Table 1 correlations and the condenser and evaporator overall heat transfer relationships as well as thermodynamic

Table 2
Output parameters of the mathematical model.

| Cooling power | W_{comp} | $W_{f,cond}$ | $W_{f,evap}$ | Heat rejection |
|-------------------|--------------------|-----------------|----------------------|----------------------|
| COP | NTU_{evap} | NTU_{cond} | ε_{evap} | ε_{cond} |
| T_c | $h_{ref,evap,in}$ | \dot{m}_{ref} | T_e | $h_g @ T_e$ |
| $h_{ref,comp,in}$ | $h_{ref,comp,out}$ | $h_g @ T_c$ | $h_f @ T_c$ | $h_{ref,TEV,in}$ |

properties correlations of HFC-134a, leads to a set of 20 coupled nonlinear equations that has to be solved simultaneously. The A/C system unknown parameters ($x_1 - x_{20}$), which are calculated using the mathematical model, are listed in Table 2.

A Newton-Raphson method is employed to develop an iterative numerical code in C for solving the set of nonlinear correlations presented in Eq. (13) [40]. In this method, the derivatives of all the equations are calculated with respect to all the unknowns and a Jacobian matrix is formed. During an iterative solution procedure, all the unknowns are calculated at any iteration (n) and used for the next iteration ($n + 1$), see Eq. (14). The iterative procedure is repeated until the maximum relative residual for all the unknown parameters becomes less than 0.001.

$$\begin{cases} g_1(x_1 = \text{Cooling power}, x_2 = W_{comp}, \dots, x_{20} = h_{ref,TEV,in}) = 0 \\ g_2(x_1 = \text{Cooling power}, x_2 = W_{comp}, \dots, x_{20} = h_{ref,TEV,in}) = 0 \\ \vdots \\ g_{20}(x_1 = \text{Cooling power}, x_2 = W_{comp}, \dots, x_{20} = h_{ref,TEV,in}) = 0 \end{cases} \quad (13)$$

$$\begin{bmatrix} x_1^{n+1} \\ \vdots \\ x_{20}^{n+1} \end{bmatrix} = \begin{bmatrix} x_1^n \\ \vdots \\ x_{20}^n \end{bmatrix} - \begin{bmatrix} \frac{\partial g_1}{\partial x_1} & \dots & \frac{\partial g_1}{\partial x_{20}} \\ \vdots & & \vdots \\ \frac{\partial g_{20}}{\partial x_1} & \dots & \frac{\partial g_{20}}{\partial x_{20}} \end{bmatrix}_{x_i^n}^{-1} \times \begin{bmatrix} g_1(x_i^n) \\ \vdots \\ g_{20}(x_i^n) \end{bmatrix} \quad (14)$$

3. Experimental setup

A new test-bed was designed and built to simulate real-time operating condition of the anti-idling truck A/C system in our lab. The test-bed should consist of two independent sources of conditioned air supply to impose any desired temperature and humidity at the air inlet to evaporator and condenser. Accordingly, for the test-bed two separate environmental chambers are required; one connected to the evaporator and the other one connected to the condenser. A schematic of the test-bed is presented in Fig. 2. The schematic shows that a number of temperature, pressure, and relative humidity sensors as well as velocity and mass flow meters are employed in the test-bed to obtain the required data.

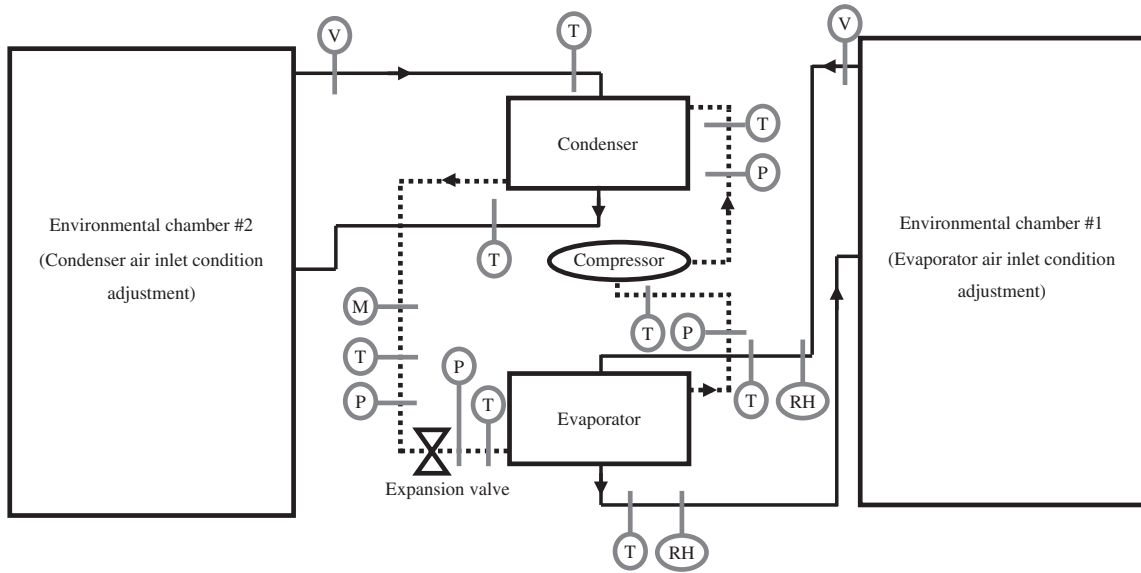


Fig. 2. Experimental setup schematic (solid lines = air flow, dashed lines = refrigerant flow, T = temperature sensor, P = pressure sensor, M = mass flow meter, V = velocity meter, RH = relative humidity sensor).

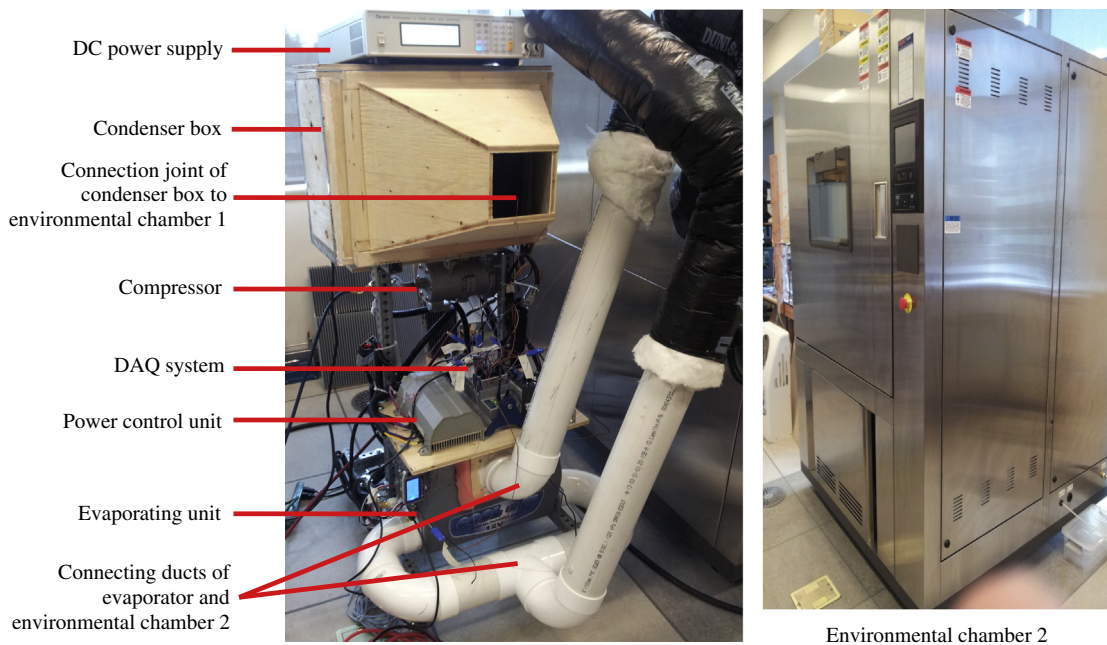


Fig. 3. Experimental setup.

A photo of the built test-bed is shown in Fig. 3. The condenser-side air duct is detached for this photo to have a better observation. The test-bed consists of an anti-idling A/C system installed on a portable base with duct connections to the environmental chambers. Booster fans are installed to compensate pressure drop in the ducting system to provide the nominal air flow rates for both the condenser and evaporator coils. T-type thermocouples from OMEGA with ± 0.1 °C accuracy are installed at 4 locations on the evaporator and condenser air streams. Moreover, two wind sensors model MD0550 with accuracy of ± 0.15 m/s from Modern Device are installed to measure the velocity for both the evaporator and condenser air flows. Additionally, two Rotronic humidity sensors model HC2-S3 with $\pm 0.8\%$ RH accuracy are installed to measure humidity at inlet and outlet of the evaporator air stream.

T-type thermocouples (from OMEGA with ± 0.1 °C accuracy) and pressure transducers model PX309 manufactured by OMEGA with 0.25% accuracy are installed at four locations of the A/C unit to measure both the high and low temperatures/pressures of the refrigerant. Micro Motion 2400S transmitter with 0.5% accuracy from Emerson Electric Co. is utilized to log the refrigerant mass flow rate. Three Chroma programmable DC power supplies model 62012P-40-120 are employed to feed and measure the power consumption of the compressor and fans. An NI instrument Data Acquisition System (DAQ), model 9184, is used to collect the input data from the thermocouples, pressure transducers, refrigerant flow meter, velocity meters, and power supplies, and send them to a computer. LabVIEW software is employed to obtain all the measured data from equipment and save them into a file. The frequency of all the measurements is 60 Hz.

4. Results and discussion

In spite of undergoing a transient ambient temperature behavior for common truck A/C systems due to movement, the anti-idling A/C system is used while the truck is not moving. Accordingly, the operating condition for the anti-idling A/C system can be assumed steady state with a good approximation. However, the ambient temperature is different from location to location and smoothly varies during the anti-idling period. Therefore, our steady state experimental and mathematical studies are carried out in a wide range of 20–60 °C for the condenser air inlet temperature and 10–50 °C for the evaporator air inlet temperature. The experiments show that it takes around one hour to arrive at steady state condition for each test, see Fig. 4. After achieving the steady state condition, average values of each parameter are utilized for the purpose of model verification and system performance analysis.

4.1. Model verification, effect of condenser air inlet temperature on COP

To verify the developed mathematical model, experimental data for a wide range of operating condition is obtained using the custom-built test-bed describe in Section 3. Condenser air inlet temperature $T_{a,cond,in}$ is one of the most effective parameters on the performance of an A/C system. Since the condenser is installed exposed to the ambient air, the $T_{a,cond,in}$ represents the ambient temperature. Fig. 5 shows a comparison between the mathematical model and experimental data for air temperature at the outlet of evaporator $T_{a,evap,out}$ in a wide range of evaporator air inlet temperature $T_{a,evap,in}$. It should be mentioned that the relative humidity of inlet air is kept at 50% for all the $T_{a,evap,in}$. Also, the evaporator and condenser air flow rates are kept at the nominal capacities that are 0.04 and 0.25 kg/s, respectively. This figure shows that even for a constant $T_{a,evap,in}$, increasing the $T_{a,cond,in}$ causes a gradual increment in the evaporator air outlet temperature $T_{a,evap,out}$. This behavior can be explained based on the condensing and evaporating temperatures of the refrigeration cycle T_c, T_e . Increasing the $T_{a,cond,in}$ directly increases the T_c in order to keep the temperature gradient for a sufficient heat rejection rate. The T_c increment leads to a higher condensing pressure P_c . Therefore, based on the compressor characteristics as a turbo-machine and the expansion valve properties, the low pressure (evaporating pressure P_e) and mass flow rate of refrigerant will change correspondingly.

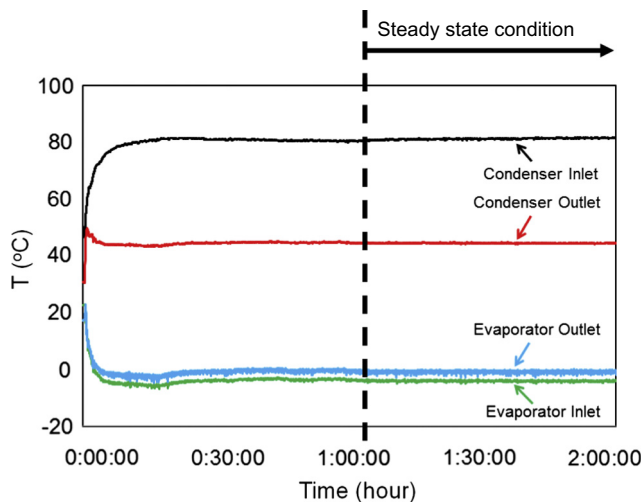


Fig. 4. Steady state condition achievement – measured refrigerant side temperature.

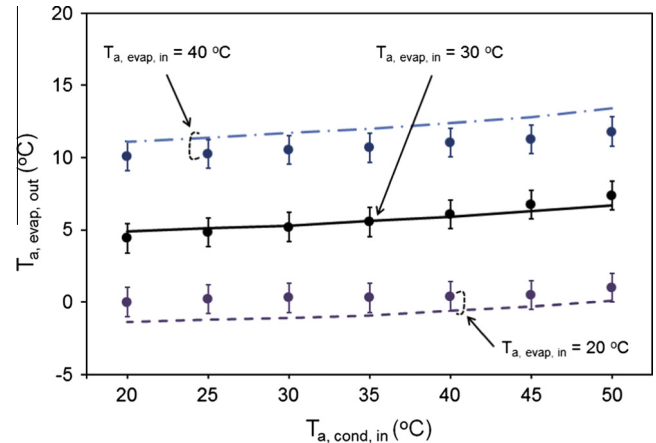


Fig. 5. Verification of the model (lines) with experimental data (symbols), evaporator air outlet temperature ($T_{a,evap,out}$) vs. condenser air inlet temperature ($T_{a,cond,in}$).

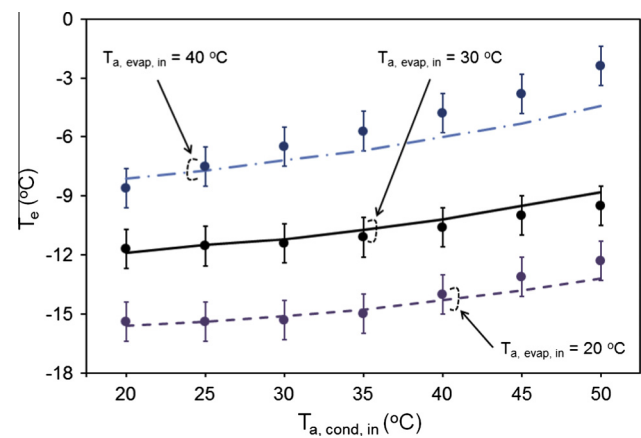


Fig. 6. Verification of the model (lines) with experimental data (symbols), Evaporating temperature (T_e) vs. condenser air inlet temperature ($T_{a,cond,in}$).

Fig. 6 presents a comparison between the mathematical model and the obtained experimental data for evaporating temperature T_e and shows that by increasing $T_{a,cond,in}$, the T_e increases and the rate of this increment is higher for a higher $T_{a,evap,in}$. Increment of T_e is due to increment of evaporating pressure P_e which comes from condensing pressure P_c enhancement due to rise of T_c .

Also, Figs. 7–10 show the behavior of refrigerant mass flow rate, total system power consumption, cooling power, and COP, respectively. Fig. 7 indicates that by increasing $T_{a,cond,in}$ for any constant $T_{a,evap,in}$, which results in increment of both T_e and T_c , the refrigerant mass flow rate increases. Additionally, for any constant $T_{a,cond,in}$, increasing $T_{a,evap,in}$ brings to an increment of refrigerant mass flow rate. The main reason of mass flow rate increment at higher $T_{a,cond,in}$ and $T_{a,evap,in}$ is the refrigerant's density increment because of higher P_c and P_e . Because the compressor operates at a same speed, it moves higher mass flow rate of refrigerant at larger P_c and P_e due to the higher density. Based on this observed behavior, one can conclude that working under warmer ambient condition, which increases both $T_{a,cond,in}$ and $T_{a,evap,in}$, leads to increment of refrigerant mass flow rate.

Due to refrigerant mass flow rate increment as well as pressure ratio changes, the total power consumption increases by increasing the $T_{a,cond,in}$, see Fig. 8. A same trend exists for $T_{a,evap,in}$ increment at any constant $T_{a,cond,in}$ that means in relatively warmer areas a

refrigeration unit draws more full-load power than in colder areas under a same duty cycle.

Furthermore, as can be observed in Fig. 9, by increasing $T_{a,cond,in}$ for any constant $T_{a,evap,in}$, the cooling capacity of the system decreases. This decrement is as a result of reduction in the air-refrigerant temperature difference due to T_e increment for a constant $T_{a,evap,in}$. However, this figure shows that for any constant $T_{a,cond,in}$,

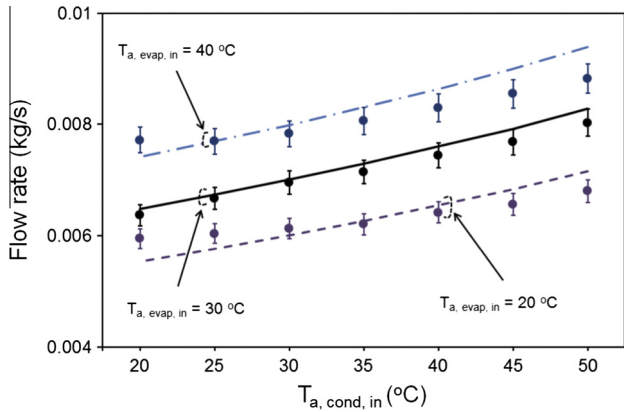


Fig. 7. Verification of the model (lines) with experimental data (symbols), refrigerant mass flow rate (\dot{m}_{ref}) vs. condenser air inlet temperature ($T_{a,cond,in}$).

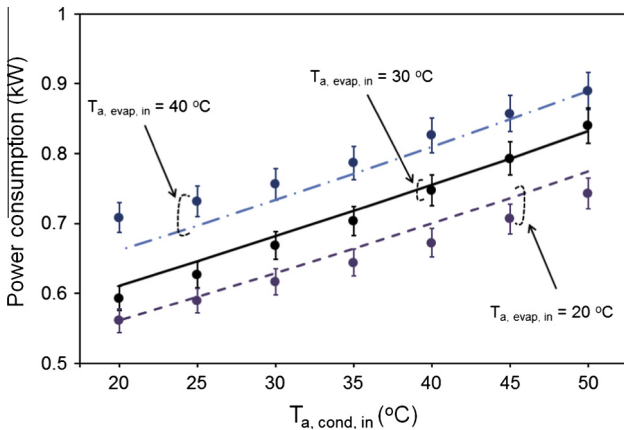


Fig. 8. Verification of the model (lines) with experimental data (symbols), total power consumption vs. condenser air inlet temperature ($T_{a,cond,in}$).

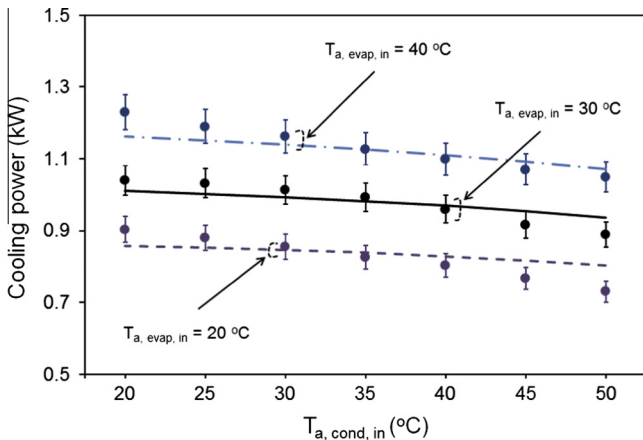


Fig. 9. Verification of the model (lines) with experimental data (symbols), cooling power vs. condenser air inlet temperature ($T_{a,cond,in}$).

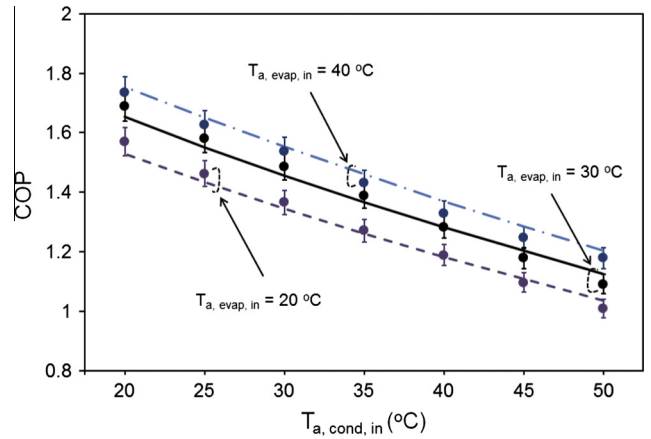


Fig. 10. Verification of the model (lines) with experimental data (symbols), COP vs. condenser air inlet temperature ($T_{a,cond,in}$).

increasing $T_{a,evap,in}$ results in a higher cooling capacity of the system. Therefore, increasing the ambient temperature (higher $T_{a,cond,in}$ and $T_{a,evap,in}$) may increase or decrease the total cooling capacity of the system depending upon the thermal insulation of the conditioned space. In other words, if the thermal insulation of the conditioned space prevents an intensive temperature rise inside the space after an intensive ambient temperature increment (increasing $T_{a,cond,in}$ for almost a constant $T_{a,evap,in}$), the cooling capacity of the system will drop. However, if a poor insulation lets the indoor temperature to increase by ambient temperature increment, the provided cooling by the system will increase though the total efficiency degrades due to higher thermal losses.

Finally, for any constant $T_{a,evap,in}$, the power consumption increment and cooling capacity decrement of the system by increasing $T_{a,cond,in}$ leads to a COP decrement that can be observed in Fig. 10. However, increasing $T_{a,evap,in}$ for any constant $T_{a,cond,in}$ slightly increases the system COP. Based on this behavior, one can conclude that increasing the thermostatic set point of the conditioned space (higher $T_{a,evap,in}$) for any ambient condition will result in a higher COP.

The maximum relative discrepancy between the model output and the measured values is 10.6% emerging from cooling load results. For the rest of the presented parameters, the maximum relative discrepancy between the modeled and the measured values is less than 10%. The main sources of relative discrepancy between the model and experimental data come from either measuring equipment (minor error – from experimental data) or sub-models (major error – from model outputs) inaccuracies. Since there are a variety of characteristic parameters existing in the sub-model correlations (dimensions of coils and fins, heat transfer properties of coil/fin material, refrigerant thermodynamics properties, convective heat transfer coefficients, etc.), which are affected by measurement or round-off errors and impurities, the model results and experimental data cannot be exactly the same. In this study, the heat exchangers characteristic given by the manufacturer especially the material properties is the main source of relative difference between the developed model and the experimental results.

4.2. Effects of condenser air flow rate on COP

To investigate the effects of condenser fan speed on the system performance, in this section a wide range of condenser air flow rate $\dot{m}_{a,cond}$ is modeled and the results are presented. In addition to partial flow rates of the existing condenser fan (33–100% of the

nominal fan capacity 0.25 kg/s), higher flow rates (100–167%) are also simulated to assess the possibility of performance improvement by replacing the existing fan with a higher capacity one. The evaporator air inlet temperature is assumed to be kept at 20 °C and the evaporator fan is set at nominal speed. Figs. 11–14 respectively represent the variations of refrigerant flow rate, total system power consumption, cooling power, and COP for the mentioned range of $\dot{m}_{a,cond}$ based on the mathematical modeling.

Fig. 11 shows that the refrigerant mass flow rate \dot{m}_{ref} continuously decreases with higher rate at smaller $\dot{m}_{a,cond}$ (less than 80% of the nominal capacity: ~ 0.2 kg/s). This decrement is due to higher heat transfer rate at larger $\dot{m}_{a,cond}$ which reduces the condensing temperature T_c and the corresponding pressure P_c . The P_c reduction results in evaporating pressure P_e decrement. Accordingly, the total refrigerant pressure in the cycle decreases and results in lower refrigerant density which brings to a lower \dot{m}_{ref} for a constant speed compressor operation. However, beyond almost 80% of the nominal $\dot{m}_{a,cond}$ (~ 0.2 kg/s) the variation of \dot{m}_{ref} becomes less sensible. This behavior is due to power consumption increment beyond the mentioned $\dot{m}_{a,cond}$, see Fig. 12, that increases the total heat rejection rate at the condenser. The increment of heat rejection basically increases T_c and negates the effect of $\dot{m}_{a,cond}$ enhancement on reducing T_c and thus, the \dot{m}_{ref} will no longer reduce remarkably.

Also, Fig. 12 indicates that by increasing $\dot{m}_{a,cond}$, the total power consumption first decreases to a point of minimum power due to predominance of compressor power reduction, then increases due to predominance of condenser fan power increment. The

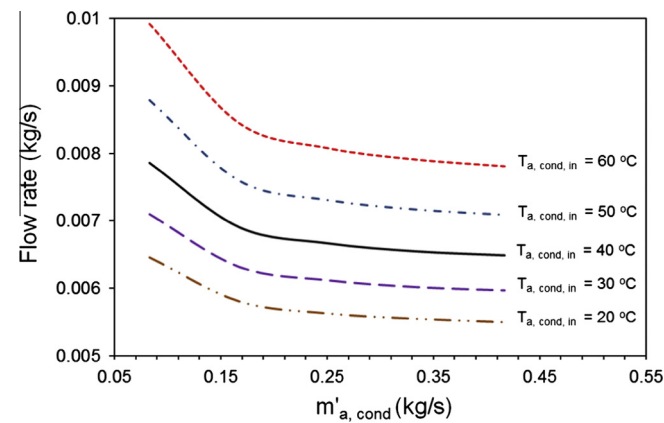


Fig. 11. Refrigerant flow rate vs. condenser air flow rate ($\dot{m}_{a,cond}$).

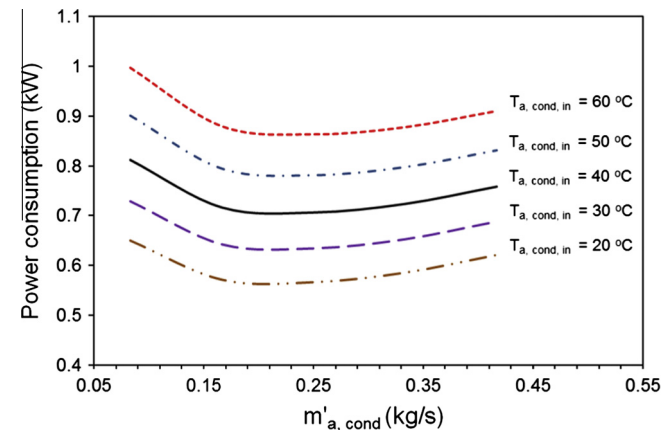


Fig. 12. Total power consumption vs. condenser air flow rate ($\dot{m}_{a,cond}$).

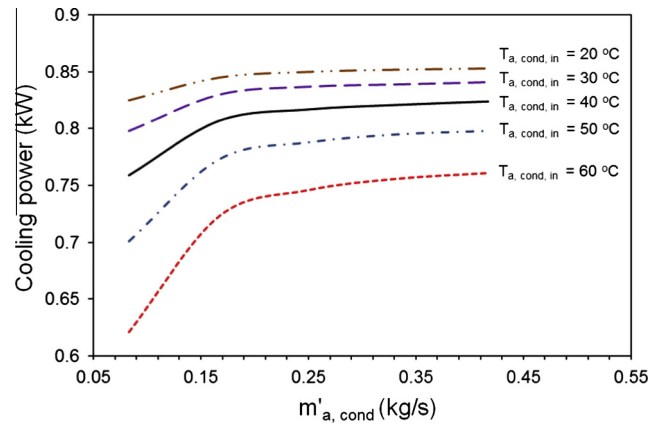


Fig. 13. Cooling power vs. condenser air flow rate ($\dot{m}_{a,cond}$).

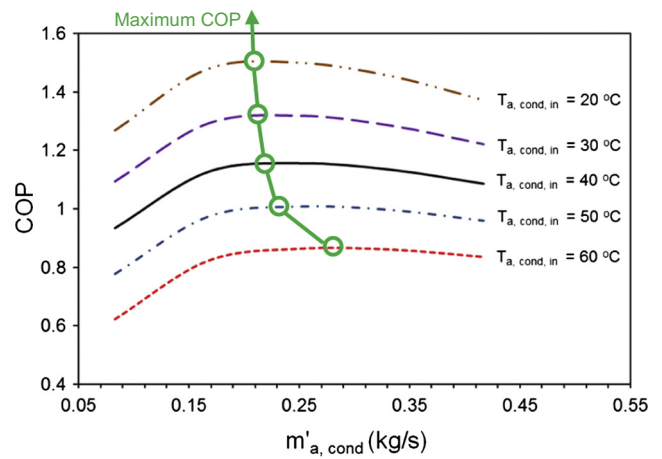


Fig. 14. COP vs. condenser air flow rate ($\dot{m}_{a,cond}$).

compressor power reduction appears due to decrement of both the refrigerant mass flow rate and cycle's high pressure. However, as the refrigerant flow rate variation becomes negligible after almost 80% of the nominal $\dot{m}_{a,cond}$, the compressor power consumption also does not change remarkably. Meanwhile, the condenser fan's power consumption continuously increases and results in total power increment.

From Fig. 13 one can conclude that the cooling power continuously increases with higher rate at smaller $\dot{m}_{a,cond}$ (less than 80% of the nominal capacity). This trend is more pronounced at higher ambient temperature. A more significant gap between the cooling power curves at higher ambient temperatures indicates a remarkable cooling capacity loss of the system in hot zones. The steeper increment of cooling power at smaller $\dot{m}_{a,cond}$ is due to more sensible reduction of T_e (as a result of T_c reduction) which increases the refrigerant-air temperature difference at evaporator. However, after almost 80% of the nominal $\dot{m}_{a,cond}$, increasing the $\dot{m}_{a,cond}$ value does not contribute to sensible changes in T_e and thus, the cooling power will no longer change sensibly.

Finally, it can be concluded from Fig. 14 that the COP first increases to a point of maximum value because of the cooling power increment and power consumption decrement, and then it starts to decrease. The decrement of COP is because of negligible increment of cooling power while the power consumption is increasing more sensibly. Therefore, due to a higher rate of power consumption increment than the cooling power growth, the COP starts to decrease. Based on this behavior, for each ambient

temperature, a point of optimum COP can be found by changing the speed of the condenser fan. Therefore, installing and using a constant speed fan for the condenser of an A/C system brings to a low COP operation for most of the duty cycle. On the flip side, equipping an A/C system to a variable speed fan for the condenser, even if it is simply controlled based on the ambient temperature, can improve the performance of the system significantly.

4.3. Effects of evaporator air flow rate on COP

Figs. 15–17 represent the behavior of total power consumption, cooling power, and COP vs. evaporator air flow rate $\dot{m}_{a, evap}$ for a wide range of ambient temperatures based on the modeling. The evaporator air inlet temperature for all of the cases is assumed to be kept at 20 °C and the condenser fan is assumed to be set at its nominal speed. Similar to the condenser air flow rate parameter in Section 4.2, in this section a wide range of 33–167% of nominal capacity is assumed for the $\dot{m}_{a, evap}$. From Figs. 15 and 16 one can conclude that both the power consumption and cooling power increase by increasing $\dot{m}_{a, evap}$ for any constant $\dot{m}_{a, cond}$ and $T_{a, cond, in}$. The cooling power increment emerged from higher heat transfer rate for larger $\dot{m}_{a, evap}$ values. Furthermore, due to increment of heat transfer rate at evaporator, the evaporating temperature and pressure will rise that brings to a higher refrigerant density. Accordingly, the compressor power consumption will increase that contributes to power consumption increment of the system. However, the cooling power increment dominates the power consumption increment that results in continuous COP enhancement

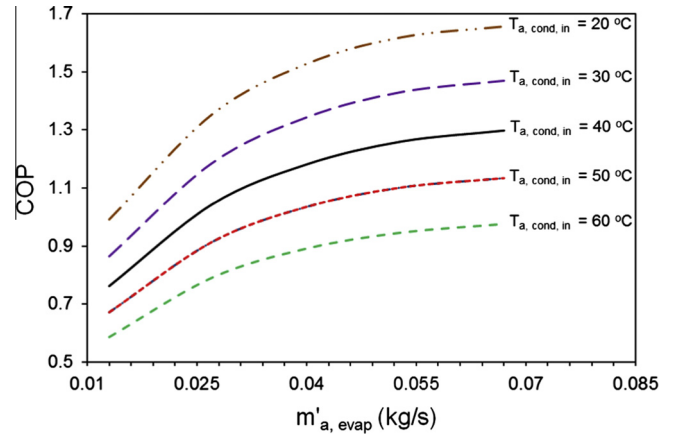


Fig. 17. COP vs. evaporator air flow rate ($\dot{m}_{a, evap}$).

by increasing $\dot{m}_{a, evap}$ for any constant $\dot{m}_{a, cond}$ and $T_{a, cond, in}$. The rate of COP increment is higher at smaller $\dot{m}_{a, evap}$. Comparing the effects of evaporator and condenser air flow rates on COP shows that although the $\dot{m}_{a, cond}$ can bring to optimum COP for the A/C system, the $\dot{m}_{a, evap}$ does not result in optimum values; however, the $\dot{m}_{a, evap}$ plays an important role in the magnitude of the system COP. In Figs. 18–20, the A/C system power consumption, cooling power, and COP for a wide range of $\dot{m}_{a, cond}$ and $\dot{m}_{a, evap}$ are presented based on modeling. The evaporator and condenser air inlet temperatures ($T_{a, evap, in}$, $T_{a, cond, in}$) are set at 26.7 and 35 °C respectively, based on ANSI/AHRI standard 210/240-2008. In addition to the mentioned $T_{a, evap, in}$, $T_{a, cond, in}$ set points, the simulations are carried out for other set points and the trends of the results are similar to the presented ones.

Fig. 18 shows that the power consumption first decreases to a point of minimum power (compressor power reduction predominancy), then starts to increase (condenser fan power increment predominancy). Furthermore, Fig. 19 shows that cooling power increases by increasing the $\dot{m}_{a, cond}$ or $\dot{m}_{a, evap}$; however, the rate of increment at smaller $\dot{m}_{a, cond}$ or $\dot{m}_{a, evap}$ is more considerable. Similar to the results of Section 4.2, this behavior is emerged from the variations of T_e , T_c , and refrigerant mass flow rate. From Fig. 20 one can conclude that for a given $T_{a, evap, in}$ and $T_{a, cond, in}$, which respectively represent the vehicle cabin temperature and the ambient temperature, and any evaporator fan speed adjustment by the truck driver, there is a point of optimum COP for the system that can be achieved by setting the condenser fan speed. The

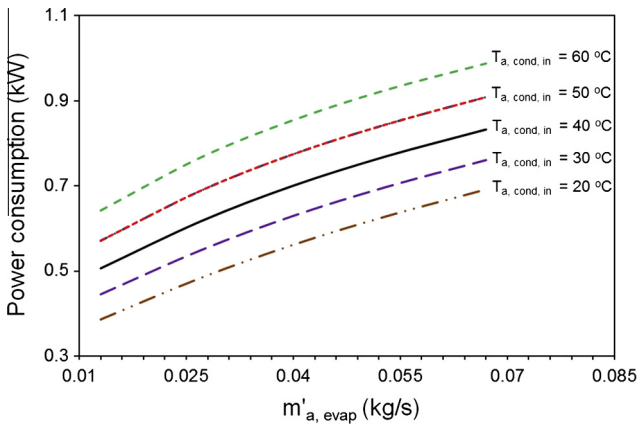


Fig. 15. Total power consumption vs. evaporator air flow rate ($\dot{m}_{a, evap}$).

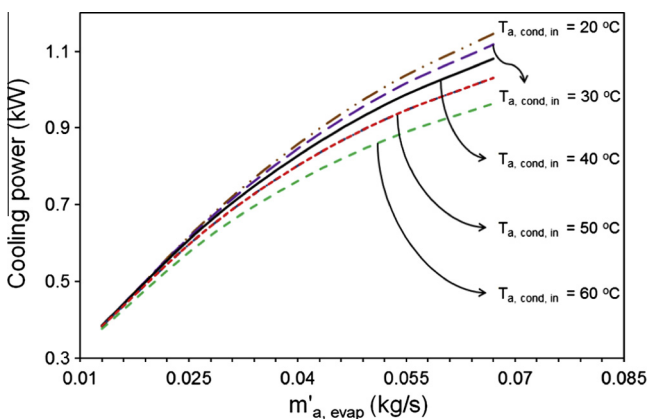


Fig. 16. Cooling power vs. evaporator air flow rate ($\dot{m}_{a, evap}$).

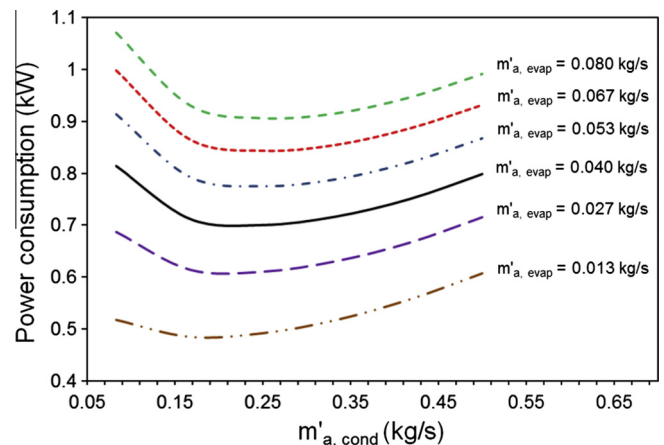


Fig. 18. Total power consumption vs. condenser and evaporator air flow rates ($\dot{m}_{a, cond}$, $\dot{m}_{a, evap}$).

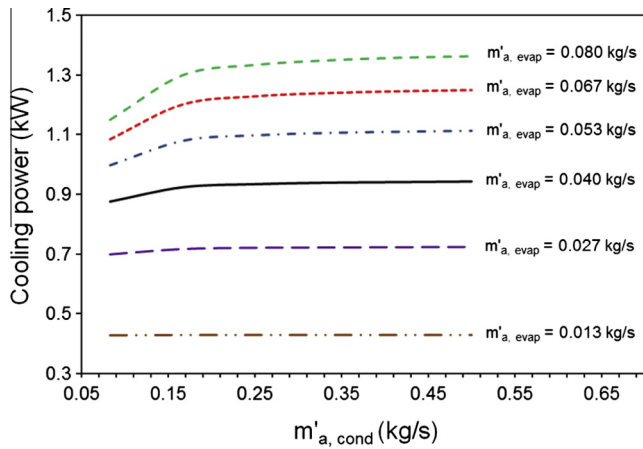


Fig. 19. Cooling power vs. condenser and evaporator air flow rates ($\dot{m}_{a,cond}$, $\dot{m}_{a,evap}$).

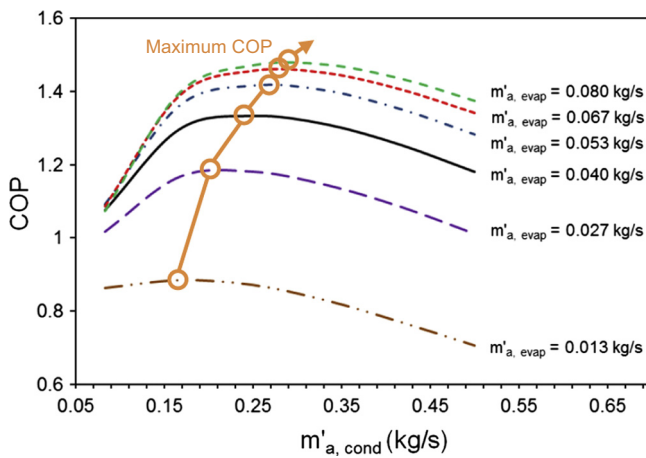


Fig. 20. COP vs. condenser and evaporator air flow rates ($\dot{m}_{a,cond}$, $\dot{m}_{a,evap}$).

magnitude of the system's optimum COP increases by increasing the $\dot{m}_{a,evap}$. Although the rate of this increment is significant at smaller $\dot{m}_{a,evap}$, it becomes nearly negligible at larger $\dot{m}_{a,evap}$. For the presented ANSI/AHRI 210/240-2008 condition, the maximum achievable COP is appeared at 200% of nominal $\dot{m}_{a,evap}$ and 125% of nominal $\dot{m}_{a,cond}$. Finally, it can be concluded that for any vehicle's cabin temperature set point ($T_{a,evap,in}$) and ambient temperature ($T_{a,cond,in}$), based on the cooling demand, which can be calculated from common heat balance methods, an appropriate $\dot{m}_{a,evap}$ can be found to satisfy the demand (referring to Fig. 19). Then, utilizing the found $\dot{m}_{a,evap}$, an optimum condenser fan speed that contributes to the maximum system COP can be obtained (referring to Fig. 20). Accordingly, the COP of A/C system can be improved by developing an intelligent control to find the optimum condenser and evaporator air flow rates for any operating condition and command the fans to provide the obtained flow rates. The obtained values showed that there is a potential of 11% improvement in the COP of system. Based on this logic, the total performance of existing truck A/C systems can be significantly improved to achieve a high level of fuel conservation by either adding or even replacing the common engine-driven units with battery-powered anti-idling A/C units equipped to the intelligent control module. Based on the introductory presented literature data on fuel consumption and GHG emission and the obtained 11% COP improvement potential, it can be concluded that for each truck at least 0.33 lit/h in fuel consumption (at most 2.3–7.6 lit/h if using of anti-idling A/C

system results in complete engine shut-off) can be saved during the idling period (average of 11 h/day for long-haul trucks) if the common A/C systems are replaced by the intelligently controlled anti-idling types. This replacement will contribute to at least 5.8 g/h, 1099 g/h, 342 g/h, 0.27 g/h, and 25 g/h respectively for HC, CO₂, CO, PM, and NO_x emissions reduction during the idling period.

5. Conclusions

This paper presented a mathematical and experimental investigation into anti-idling A/C system for trucks. One of the recently developed battery-powered anti-idling A/C systems was employed to build a test-bed. A new mathematical model, which simulated the thermodynamic and heat transfer characteristics of the A/C systems based on the component sub-models, was developed. Various temperature, pressure, electric power, and flow rate measuring devices were utilized in the test-bed to collect real-time data for the mathematical model verification. Using the test results for a wide range of operating conditions, accuracy of the mathematical model was verified with a maximum relative discrepancy of 10.6%. Utilizing the verified model, a comprehensive study on different parameters of the anti-idling A/C system including: condenser air inlet temperature $T_{a,cond,in}$ (represents the ambient temperature), evaporator air inlet temperature $T_{a,evap,in}$ (represents the air conditioned space temperature), condenser air flow rate $\dot{m}_{a,cond}$, and evaporator air flow rate $\dot{m}_{a,evap}$, was carried out. The followings were mainly concluded from the parametric study:

- Increasing $T_{a,cond,in}$ for any constant $T_{a,evap,in}$ leads to decrement of the system COP due to the cooling power reduction and power consumption increment.
- Increasing $\dot{m}_{a,cond}$, which represents the condenser fan speed increment, for any constant $T_{a,cond,in}$ increases the cooling power of the system. The rate of cooling power increment is significant at lower $\dot{m}_{a,cond}$; however, it becomes slighter at higher $\dot{m}_{a,cond}$. Also, by increasing $\dot{m}_{a,cond}$, due to continuous decrement of the compressor power consumption while the condenser fan power consumption increases, the total power consumption first decreases at lower $\dot{m}_{a,cond}$ and then increases at higher $\dot{m}_{a,cond}$. Consequently, the COP first increases at lower $\dot{m}_{a,cond}$ and then decreases at higher $\dot{m}_{a,cond}$ that leaves a point of optimum COP for the system.
- Increasing $\dot{m}_{a,evap}$, which represents the evaporator fan speed increment, for any constant $T_{a,cond,in}$ increases the cooling power, total power consumption, and COP of the system. The rate of these increments is more significant at lower $\dot{m}_{a,evap}$.
- Increasing $\dot{m}_{a,cond}$ for any constant $\dot{m}_{a,evap}$ slightly increases the cooling power of the system. However, the total power consumption first decreases at lower $\dot{m}_{a,cond}$ and then increases at higher $\dot{m}_{a,cond}$. Eventually, the COP first increase and then decreases that leaves a point of optimum COP for the system.
- It was concluded that for any vehicle's cabin temperature set point, ambient temperature, and cooling demand, the appropriate evaporator and condenser fan speeds can be found that brings to an optimum COP for the system (at least 11% improvement in COP). Based on the obtained results, if an intelligently controlled anti-idling A/C system is added to a truck to perform only during the idling period, at least 0.33 lit/h in fuel consumption (at most 2.3–7.6 lit/h if using of anti-idling A/C system results in complete engine shut-off) and 5.8 g/h, 1099 g/h, 342 g/h, 0.27 g/h, and 25 g/h respectively for HC, CO₂, CO, PM, and NO_x emissions can be reduced.

Acknowledgements

This work was supported by Automotive Partnership Canada (APC), Grant No. APCPJ 401826-10. The authors would like to thank kind support from the Cool-It Group, #100 – 663 Sumas Way, Abbotsford, BC, Canada.

References

- [1] Stodolsky F, Gaines L, Vyas A. Analysis of technology options to reduce the fuel consumption of idling trucks. Center for Transportation Research, Argonne National Laboratory, U.S. Department of Energy; 2000.
- [2] Gaines L, Rask E, Keller G. Which is greener: idle, or stop and restart? Comparing fuel use and emissions for short passenger car stops. Argonne National Laboratory, U.S. Department of Energy; 2012.
- [3] Rahman SMA, Masjuki HH, Kalam Ma, Abedin MJ, Sanjid a, Sajjad H. Impact of idling on fuel consumption and exhaust emissions and available idle-reduction technologies for diesel vehicles – a review. *Energy Convers Manage* 2013;74:171–82.
- [4] Tian C, Li X. Numerical simulation on performance band of automotive air conditioning system with a variable displacement compressor. *Energy Convers Manage* 2005;46:2718–38.
- [5] Brodrick C-J, Dwyer Ha, Farshchi M, Harris DB, King FG. Effects of engine speed and accessory load on idling emissions from heavy-duty diesel truck engines. *J Air Waste Manage Assoc* 2002;52:1026–31.
- [6] Ji C, Liang C, Zhu Y, Liu X, Gao B. Investigation on idle performance of a spark-ignited ethanol engine with dimethyl ether addition. *Fuel Process Technol* 2012;94:94–100.
- [7] Gaines L. Idling reduction for medium-duty fleets. In: *Green Fleets Conf.*, Schaumburg; 2012.
- [8] Farrington R, Rugh J. Impact of vehicle air-conditioning on fuel economy, tailpipe emissions, and electric vehicle range preprint; 2000.
- [9] Clark NN, Gautam M, Wayne WS, Lyons DW, Thompson G. California heavy-duty diesel truck emissions characterization for project #-55/59 phase 1.5; 2004.
- [10] Ryska A. Fuel consumption of vehicle powered refrigeration units; 2007.
- [11] Caterpillar, Understanding tractor-trailer performance; 2006.
- [12] Cantoria CS, Arnold P. Putting a stop to car idling: emissions worsen global warming conditions; 2012.
- [13] MacDonald C, Douglas R, Tamayol A, Bahrami M. A feasibility study of auxiliary HVAC systems for reducing idling time of long haul trucks. In: *Proc. ASME 2012 Summer Heat Transf. Conf. HT2012*, Asme, Rio Grande; 2012.
- [14] Afram A, Janabi-Sharifi F. Review of modeling methods for HVAC systems. *Appl Therm Eng* 2014;67:507–19.
- [15] Anand S, Gupta a, Tyagi SK. Simulation studies of refrigeration cycles: a review. *Renew Sustain Energy Rev* 2013;17:260–77.
- [16] Ding G. Recent developments in simulation techniques for vapour-compression refrigeration systems. *Int J Refrig* 2007;30:1119–33.
- [17] Hermes CJL, Melo C, Knabben FT, Gonçalves JM. Prediction of the energy consumption of household refrigerators and freezers via steady-state simulation. *Appl Energy* 2009;86:1311–9.
- [18] Boeng J, Melo C. Mapping the energy consumption of household refrigerators by varying the refrigerant charge and the expansion restriction. *Int J Refrig* 2014;41:37–44.
- [19] Lee GH, Yoo JY. Performance analysis and simulation of automobile air conditioning system. *Int J Refrig* 2000;23:243–54.
- [20] Cho H, Lee H, Park C. Performance characteristics of an automobile air conditioning system with internal heat exchanger using refrigerant R1234yf. *Appl Therm Eng* 2013;61:563–9.
- [21] Joudi Ka, Mohammed ASK, Aljanabi MK. Experimental and computer performance study of an automotive air conditioning system with alternative refrigerants. *Energy Convers Manage* 2003;44:2959–76.
- [22] Han XH, Li P, Xu YJ, Zhang YJ, Wang Q, Chen GM. Cycle performances of the mixture HFC-161 + HFC-134a as the substitution of HFC-134a in automotive air conditioning systems. *Int J Refrig* 2013;36:913–20.
- [23] Yoo SY, Lee DW. Experimental study on performance of automotive air conditioning system using R-152a refrigerant. *Int J Automot Technol* 2009;10:313–20.
- [24] Brown JS, Yana-motta SF, Domanski PA. Comparative analysis of an automotive air conditioning systems operating with CO₂ and R134a 25. *Int J Refrig* 2002:19–32.
- [25] Ratts EB, Brown JS. An experimental analysis of cycling in an automotive air conditioning system. *Appl Therm Eng* 2000;20:1039–58.
- [26] Wang S, Gu J, Dickson T, Dexter J, McGregor I. Vapor quality and performance of an automotive air conditioning system. *Exp Therm Fluid Sci* 2005;30:59–66.
- [27] Macagnan MH, Copetti JB, Souza RB, Reichert RK, Amaro M. Analysis of the influence of refrigerant charge and compressor duty cycle in an automotive air conditioning system. In: *22nd Int. Congr. Mech. Eng. (COBEM 2013)*; 2013. p. 6151–61.
- [28] Alkan A, Hosoz M. Comparative performance of an automotive air conditioning system using fixed and variable capacity compressors. *Int J Refrig* 2010;33:487–95.
- [29] Jabardo JMS, Mamani WG, Ianella MR. Modeling and experimental evaluation of an automotive air conditioning system with a variable capacity compressor. *Int J Refrig* 2002;25:1157–72.
- [30] Sharafian A, Bahrami M. Assessment of adsorber bed designs in waste-heat driven adsorption cooling systems for vehicle air conditioning and refrigeration. *Renew Sustain Energy Rev* 2014;30:440–51.
- [31] Rêgo aT, Hanriot SM, Oliveira aF, Brito P, Rêgo TFFU. Automotive exhaust gas flow control for an ammonia–water absorption refrigeration system. *Appl Therm Eng* 2014;64:101–7.
- [32] Li J, Xu S. The performance of absorption–compression hybrid refrigeration driven by waste heat and power from coach engine. *Appl Therm Eng* 2013;61:747–55.
- [33] Zheng W, Chen Y, Hua N, Zhong T, Gong Y. Comparative performance of an automotive air conditioning system using micro-channel condensers with and without liquid–vapor separation. *Energy Proc* 2014;61:1646–9.
- [34] Muller C. New reversible air-conditioning magnetocaloric system, environmentally friendly and highly energy efficient, SAE Tech. Pap. No. 2009-01-0313. (n.d.).
- [35] Gould D. Theoretical analysis of the steam pressure exchange ejector for an automotive air conditioning application. University of Vermont; 2009.
- [36] Ünal Ş, Yilmaz T. Thermodynamic analysis of the two-phase ejector air-conditioning system for buses. *Appl Therm Eng* 2015.
- [37] Jolly PG, Tso CP, Wong YW, Ng SM. Simulation and measurement on the full-load performance of a refrigeration system in a shipping container. *Int J Refrig* 2000;23:112–26.
- [38] Shah RK, Sekulic DP. Fundamentals of heat exchanger design. John Wiley & Sons; 2003.
- [39] Zhao L, Cai W, Ding X, Chang W. Model-based optimization for vapor compression refrigeration cycle. *Energy* 2013;55:392–402.
- [40] Abbasbandy S. Improving Newton–Raphson method for nonlinear equations by modified Adomian decomposition method. *Appl Math Comput* 2003;145:887–93.